

# Cool-contacts: Cryo-Electron Microscopy of Membrane Contact Sites and Their Components

Contact  
Volume 7: 1–14  
© The Author(s) 2024  
Article reuse guidelines:  
sagepub.com/journals-permissions  
DOI: 10.1177/  
25152564241231364  
journals.sagepub.com/home/ctc



Cyan Ching<sup>1</sup> , Julien Maufront<sup>1</sup>, Aurélie di Cicco<sup>1</sup>, Daniel Lévy<sup>1</sup> ,  
and Manuela Dezi<sup>1</sup> 

## Abstract

Electron microscopy has played a pivotal role in elucidating the ultrastructure of membrane contact sites between cellular organelles. The advent of cryo-electron microscopy has ushered in the ability to determine atomic models of constituent proteins or protein complexes within sites of membrane contact through single particle analysis. Furthermore, it enables the visualization of the three-dimensional architecture of membrane contact sites, encompassing numerous copies of proteins, whether in vitro reconstituted or directly observed in situ using cryo-electron tomography. Nevertheless, there exists a scarcity of cryo-electron microscopy studies focused on the site of membrane contact and their constitutive proteins. This review provides an overview of the contributions made by cryo-electron microscopy to our understanding of membrane contact sites, outlines the associated limitations, and explores prospects in this field.

## Keywords

Cryo-electron microscopy, membrane contact sites, cryo-electron tomography, structure, lipid transfer protein

## Introduction

Membrane contact sites (MCS) are cellular regions where two organelles come into proximity, facilitated by specific proteins that not only create a physical connection but also serve distinct functions like lipid transport, calcium signaling, or organelle inheritance. These MCS are found between the endoplasmic reticulum (ER) and various organelles, as well as between different organelles other than the ER. They exhibit diversity in their shapes, compositions, and dynamics, with intermembrane gaps spanning from 10 to 45 nm across, up to several hundreds of nanometers. The duration of MCS existence varies, typically lasting from seconds to a few hours (Eisenberg-Bord et al., 2016; Scorrano et al., 2019).

Proteins found within MCS can exist as single polypeptide chains or as complexes comprising multiple proteins. These proteins may be monomeric, multimeric, or heteromeric in nature. They typically possess specific domains that bind to membranes of organelles, or they may feature transmembrane domains. While atomic models of certain subdomains within these proteins, such as lipid translocating domains or membrane binding domains, have been established through X-ray crystallography, comprehensive atomic models of complete MCS proteins, whether on its own or associated with membranes, remain absent.

In the study of MCS, electron microscopy (EM) has played and continues to play a crucial role. This imaging technique, capable of capturing images containing information from the atomic to microns scale, aligns well with the dimensions of MCS. The discovery and initial imaging of MCS date back to 1956 (Bernhard and Rouiller, 1956). Subsequently, advancements in technology have greatly benefited the investigation of MCS. These include the use of chemical agents for sample fixation to enable MCS visualization (Mesmin et al., 2013; Venditti et al., 2019), high-pressure freezing and freeze substitution for better preservation of organelle ultrastructure and inter-organelle spaces (Di Mattia et al., 2018), electron tomography (ET) to achieve three-dimensional (3D) visualization of MCS (Daniele

<sup>1</sup>Institut Curie, Université PSL, Sorbonne Université, CNRS UMR168, Laboratoire Physique des Cellules et Cancer, Paris, France

Received September 29, 2023 Accepted January 23, 2024.

## Corresponding Authors:

Daniel Lévy, Institut Curie, Université PSL, Sorbonne Université, CNRS UMR168, Laboratoire Physique des Cellules et Cancer, 75005 Paris, France.  
Email: daniel.levy@curie.fr

Manuela Dezi, Institut Curie, Université PSL, Sorbonne Université, CNRS UMR168, Laboratoire Physique des Cellules et Cancer, 75005 Paris, France.  
Email: manuela.dezi@curie.fr



et al., 2014; Hoffmann et al., 2021), the identification of MCS components through immunolabeling techniques (Daniele et al., 2014; Guyard et al., 2022), and more recently, the adoption of correlative-light EM (CLEM) approaches for imaging MCS at different scales (Ganeva and Kukulski, 2020).

Unlike traditional EM, cryo-EM captures samples in vitrified ice at cryogenic temperatures with physiological solutions, preserving biological structures without fixation. This technique enables near-atomic resolution visualization of molecular structures in their natural states and surroundings. Key developments, including the introduction of direct electron detectors, other hardware improvements, more robust sample preparation methods, and powerful computational methods for processing cryo-EM data, have collectively revolutionized cryo-EM resolution (Saibil, 2022). This revolution now makes it feasible to determine the structures of proteins that were once nearly impossible to resolve, such as membrane proteins, which are notoriously challenging to crystallize. Additionally, cryo-EM enables the characterization of the 3D architectures of protein assemblies on membranes, both in vitro (e.g., ESCRTIII, COPII, and COPI complexes) (Bertin et al., 2020; Hutchings et al., 2021; Kovtun et al., 2018) and directly within their native cellular environment (Pfeffer and Mahamid, 2018; Young and Villa, 2023) through cryo-ET. These advancements have opened new avenues for the observation of MCS in increasing resolution and clarity.

Despite the potential of cryo-EM, its application in the study of MCS remains relatively limited, as evidenced by only a handful of published studies (Bieber et al., 2022; Cai et al., 2022; Collado et al., 2019; de la Mora et al., 2021; Fernández-Busnadiego, Saheki and De Camilli, 2015; Hoffmann et al., 2019; Li et al., 2023; 2020; Subra et al., 2023; Valverde et al., 2019; Wang et al., 2023; Wozny et al., 2023). In this review, we elucidate the foundational principles of cryo-EM, emphasize the distinct characteristics of MCS components, and delve into the fresh insights garnered through cryo-EM-based analysis, with a specific emphasis on MCS proteins involved in lipid transport (Tables 1 and 2).

## Cryo-EM-Single Particle Analysis of Proteins

The principle of single particle analysis (SPA) for determining atomic protein models is as follows: purified proteins are rapidly frozen in liquid ethane or an ethane-propane mixture, resulting in vitreous ice formation that maintains the sample in a native-like state that remains transparent to electrons. The image processing workflow involves multiple major steps, including the selection of two-dimensional (2D) projections of proteins (ranging from 10,000 to several million), classification, averaging to enhance the signal-to-noise

ratio, and computation of 3D models based on these classes, followed by model refinement. The resolution achieved largely depends on protein size (larger proteins yield better visibility and classification), conformational homogeneity, and the absence of flexible domains (Table 1).

SPA's strength lies in its ability to analyze proteins within their physiological buffers. Advanced 3D classification techniques allow for the identification of various coexisting conformations within a protein sample. Remarkably, SPA can achieve resolutions as high as 1.15 Å, enabling the visualization of water molecules and ions within structures like apoferritin. For smaller proteins in the range of 50–100 kDa, the use of nanobodies or megabodies can extend their size, facilitating the determination of 3D atomic models by SPA (Uchański et al., 2021), even though crystallization might still be the more straightforward method. It is important to note that 3D models can be constructed at varying resolutions, with higher resolutions for structured regions and lower resolutions for more flexible protein regions. However, highly flexible regions present challenges in structural characterization using SPA, necessitating supplementary data from techniques such as magnetic resonance and scattering techniques, single-molecule fluorescence, and molecular dynamics for a comprehensive interpretation (Yu et al., 2023).

## Structure Determination of MCS Proteins by Single Particle Analysis: VPS13 and ATG2

SPA has been applied to gain structural insights into VPS13 and proteins involved in the formation of autophagosomes, the Autophagy related (ATG) proteins like ATG2 (Table 2). VPS13 proteins (A-D) are notably large, ranging from 300–500 kDa. They play pivotal roles in lipid transport between the ER and various membranes, including those of mitochondria, the endo/lysosomal system, or lipid droplets. VPS13 comprises an N-terminus chorein domain, an FFAT motif for binding Vesicle-Associated Membrane Protein-Associated Protein (VAP), and an ER-embedded protein. Furthermore, it encompasses C-terminal adaptor domains, as well as a VAB domain and a pleckstrin homology (PH) domain that facilitate specific binding to the membranes of opposing organelles (Adlakha et al., 2022).

The structure of the N-terminal 1-1390 fragment of *C. thermophilum*'s VPS13 was elucidated by means of SPA at a resolution of 3.75 Å (Li et al., 2020). This structure, approximately 160 Å in length and primarily composed of  $\beta$  strands, takes on an open-ended basket-like appearance. However, due to limited resolution, constructing an atomic model from this data required additional complementary experiments for proper interpretation. Fortunately, an atomic crystallographic structure of the 1-335 fragment is available, and it reveals a scoop-shaped configuration with a concave surface lined by hydrophobic residues. When

**Table 1.** Principal Characteristics of Structural Analysis of Proteins by Cryo-Electron Microscopy and SPA and by Cryo-ET and STA.

Cryo-EM method	Protein	Membrane mimicking model	Images analysis	Examples of protein model and resolution from EMDB data bank.	Comments
SPA	Soluble and transmembrane proteins, filaments, nucleoproteins Viral-like particles Protein > 50–75 Kda complete protein with post-translational modifications <b>proteins involved in membrane contact sites proteins</b>	Micelles of detergent Amphiphilic polymers (SMA, Amphipols, saponins) Peptidiscs Lipid nanodisc Small lipid vesicles	10, 000- 3 million particles Several free access software including RELION Cryo-SPARC	1.15 Å resolution model of apoferritin. Highest resolution model by SPA In the EMDB data bank, resolution and % of 3D models of protein at xÅ resolution < 2 Å; 0.7% >2 Å and <3 Å; 14.2% >3 Å and <4 Å; 37.7% 1.15 Å resolution model of apoferritin. Highest resolution model by SPA EMD-11668, (Yip et al., 2020) 2.3 Å resolution model of apoferritin <i>EMD-11603</i> , (Tegunov et al., 2021) 2.9 Å resolution model of Equine Virus-like particle, EMD-14031,(Obr et al., 2022) 3.8 Å resolution model of COPII inner coat on tubular membranes, EMD-15949, (Zivanov et al., 2022a) 12 Å resolution model of mouse serotonin receptor in liposomes, <i>EMD-3108</i> , (Kudryashev et al., 2016) 4.6 Å resolution model of ribosomes on ER-vesicles, <i>EMD-15872</i> , (Gemmer et al., 2023) 8.9 Å resolution model of Ryanodine receptor in ER vesicles <i>EMD-17272</i> (Balyaschew et al., 2023)	For 3D determination at atomic resolution of proteins in different conformation and with activators, inhibitors, or cofactors Developments in deep learning for images analysis, time-resolved cryo-EM, correlation with other structural and dynamics methods SPA is sensitive to conformational heterogeneity and disordered regions
Cryo-ET and Sub-Tomogram Averaging of in vitro systems	Membrane bound and transmembrane proteins Ribosomes Large membrane complexes Viral-like particles <b>In vitro reconstituted membrane contact sites</b>	Lipid vesicles Lipid tubes Proteo-liposomes	Several free access software for 3D reconstruction of cryo-tomograms including IMOD Several free access software for subtomogram averaging including PEET, DYNAMO, EMclarity RELION 1000–100,000 sub-volume to be averaged Need expertise for STA	3D architecture of proteins assemblies, proteins assemblies on membrane Analysis of heterogeneous assemblies of proteins 3D view from molecular to micron scale Unambiguous assignment of a function from purified protein. Tuneable parameters in a simpler way than in cell Large number of molecules of proteins to determine 3D models at sub-nanometric resolution by STA	
Cryo-ET of purified organelles	Ribosomes on ER-vesicles Ryanodin receptor on ER vesicles Mitofusin on Mitochondria	Purified organelles			3D architecture of proteins in a purified organelle Large number of molecules of proteins to determine 3D models at sub-nanometric resolution by STA

(continued)

Table 1. Continued.

Cryo-EM method	Protein	Membrane mimicking model	Images analysis	Examples of protein model and resolution from EMDB data bank.	Comments
Cryo-ET edge of cell	Large proteins > 200 Kda Plasma membrane proteins Bacterial secretion systems Viruses entry/egress from cells	Edge of cell Native environment Interior of cell		3.5 Å resolution model of <i>C. crescentus</i> S layer EMD-16183, (Zivanov et al., 2022a) 26.6 Å model of platelet integrins, EMD-12285, (Sorrentino et al., 2021)	3D architecture of protein in a cellular context Need methods for proteins assignment in the cryo-tomograms e.g., cryo-CLEM, deletion of proteins with related function and expression of the proteins of interest, different protein constructs
In situ Cryo-ET after Cryo-FIB milling	<b>ER-PM membrane contact sites</b> Large proteins > 200 Kda Ribosomes Filament, microtubules, Nuclear pores Membrane-bound complexes Proteasomes Viruses in cells <b>Membrane contact sites</b>			2.9 Å resolution model of ribosome (Cheng et al., 2023)* 3.1 Å resolution model of ribosome., EMD-16721, (Xing et al., 2023) 4.5 Å nebulin bound to actin filament in skeletal sarcomere, EMD-13990, (Wang et al., 2022) 6.5 Å resolution model of mumps virus nucleocapsid in HeLa cells, EMD-13133, (Zhang et al., 2023)	Low number of copies of proteins for STA (< 10 000) Software used to identify target particles in cryo-tomogram often requires specific adaptations to the type of object to be analyzed. Lack of automated tools for particle picking can be problematic for certain target proteins, such as: • Tightly stacked filaments • Small proteins with weak signals • Heterogeneously curved filaments STA is sensitive to conformational heterogeneity and disordered regions

Examples of Proteins and Statistics are Found in the EMDB Data Bank (<https://www.ebi.ac.uk/emdb/>). SPA: single particle analysis; Cryo-ET: cryo-electron tomography; STA: sub-tomogram averaging; 3D: three-dimensional.

\* Article in BioRxiv, 3D models will be released upon publication.

fitting this fragment into the 1-1390 EM map, it became evident that the hydrophobic residues of 1-335 were oriented towards the interior of the 1-1390 fragment. Given that the 1-1390  $\beta$  strands alternate between hydrophilic and hydrophobic residues, this fitting implies that the hydrophobic groove extends along the entire length of the long fragment. Furthermore, investigations into a 1-1350 fragment of VPS13A from *S. cerevisiae* demonstrated its copurification with 10 lipid-bound molecules and its ability to facilitate lipid transfer between vesicles in the in vitro assays.

Biogenesis of autophagosomes, double-membrane vesicles formed for nutrient recycling through organelle and macromolecule degradation, involves several proteins from the ATG family. Wang et al. present high-resolution cryo-EM structures of ATG2A-WIPI4 and ATG9A-ATG2A-WIPI4 complexes at 3.23 Å and 7 Å, respectively (Wang et al., 2023). ATG2A is constituted by a hydrophobic cavity that may facilitate rapid lipid transfer and a flexible N-terminal domain, involved in the extraction and transfer of lipids for phagophore expansion. Cryo-ET of ATG9-ATG2A-WIPI4 complex between two apposed vesicles revealed variable orientation of ATG2A. A proposed model of lipids transferred from ATG9A containing vesicle to phagophore is proposed where the scramblase function of ATG9 potentially drives unidirectional lipid transfer. VPS13 and ATG2 have been visualized through in situ cryo-ET of ER/endo/lysosome (Cai et al., 2022) and ER-autophagosome (Bieber et al., 2022) MCSs, respectively.

SPA is a valuable approach for uncovering the 3D structure of MCS proteins; however, it necessitates considerations tailored to the peculiarities of MCS proteins:

- i. Knowledge gaps exist concerning the expression, purification, and functional analysis of these proteins, which are prerequisites for achieving optimal cryo-EM grid preparation in SPA. While functional subdomains of proteins have undergone extensive investigation, only a few MCS proteins, including the oxysterol-binding protein (OSBP), VAP-A, ATG2, extended-synaptotagmin proteins and tricalbins, have undergone successful purification and functional characterization. The expression of large MCS proteins like VPS13 or those with multi-span transmembrane domains, such as PTPIP51 or START3, may present challenges when attempting to express them in *E. coli*. Moreover, many MCS proteins form complex assemblies, such as VAPs with their partner proteins and the four-protein ERMES complex. MCS proteins can also exist as heterodimers, as suggested for tricalbins and extended-synaptotagmin (Fernández-Busnadiego et al., 2015; Hoffmann et al., 2019). Consequently, the purification of multiple proteins and the identification of conditions that facilitate stable complex formation are required. Fortunately, various tools in molecular biology and membrane biochemistry, including human cell
- expression, cell-free expression, and the use of polycistronic plasmids, have become accessible for purifying a wider array of MCS proteins (Kaipa et al., 2023; Sari et al., 2016). Furthermore, SPA demands substantially smaller protein quantities than X-ray crystallography, allowing for the analysis of even partially purified proteins.
- ii. MCS proteins frequently incorporate predicted disordered domains, which introduce heightened conformational variability to these proteins. This variability poses challenges when aligning and averaging protein images, ultimately diminishing the local resolution of 3D models. Intriguingly, these disordered domains often play vital roles in the proteins' functionality. For example, numerous OSBP-related proteins feature a predicted intrinsically disordered N-terminal domain, which facilitates their diffusion to the organelle surface (Jamecna et al., 2019). Similarly, VAP-A includes two flexible domains, spanning 32 and 24 amino acids, flanking its coiled-coil domain. These flexible domains are essential for tailoring VAP-A's geometry to the organization of MCS and meeting the temporal constraints of complexes (Subra et al., 2023). Even highly structured complexes like the ERMES complex exhibit flexible interfaces, likely designed to facilitate lipid diffusion (Wozny et al., 2023). Researchers can now engineer proteins with shorter flexible domains while preserving their key functional properties. For instance, in the case of VAP-A, reducing the linkers between the central coiled-coil region maintained its partner recognition capabilities and yielded higher-resolution cryo-EM images (Subra et al., 2023). Furthermore, advancements in deep learning and novel algorithms for 3D classification are poised to support this approach, enabling the analysis of millions of particles and the construction of 3D models representing various protein conformations (Saibil, 2022).
- iii. Little is known about the role of membranes in the structural organization of MCS proteins. Notably, while transmembrane domains play a crucial role in the structure of transmembrane proteins, such as facilitating interactions required for dimerization of VAPs, membrane-binding domains are equally vital components. These domains contribute to oligomeric stabilization or the recruitment of protein partners, exemplified by the interaction between the small G-protein Arf1 and the PH domain of OSBP (Mesmin et al., 2013). To unravel the structural details of transmembrane proteins in a lipid bilayer or proteins bound to a lipid ligand integrated into the lipid bilayer, researchers frequently turn to discoidal membrane patches scaffolded by apolipoprotein A1 derivatives, commonly known as lipid nanodiscs. These nanodiscs range in diameter from 7 to 20 nm

and serve as valuable tools for structural investigations (Notti and Walz, 2022). Moreover, the application of SPA has allowed the determination of the structure of the tripartite multidrug efflux systems of Gram-negative bacteria confined between two nanodiscs. This system holds promise as a tool for mimicking a tethering complex between two membranes (Daury et al., 2016). Finally, some lipid transfer proteins such as ATG2, ATG9, and Tricalbins prefer high curvature regions, which should be considered for setting up SPA experiments (Collado et al., 2019; Hoffmann et al., 2019; Wang et al., 2023).

## Cryo-ET of Membrane Contact Sites

Cryo-ET involves capturing a sequence of images of a specific object, acquired at various tilt angles within the microscope, and subsequently aligning these images to reconstruct a comprehensive 3D model of the object. The objects of interest can encompass a wide range, from individual proteins, protein assemblies, viruses, organelles, bacteria, to cells and tissues. Subsequently, a series of image processing steps comprised of image pre-processing, which serves to enhance these images for the following identification of target structures and proteins, then subtomogram averaging (STA) is performed to extract, align, and average a substantial number of sub-volumes of the tomograms, typically ranging from 1000 to 100,000. These sub-volumes contain protein domains or even complete proteins. Through an iterative process involving classification and averaging approaches, akin to those used in SPA, but applied to volumes instead, detailed 3D models of the proteins can be determined. Once these molecular models are obtained, they can be back-projected into the original tomograms, providing insights into the larger-scale distribution of these proteins within their biological context, whether in vitro reconstructed or in situ (Castaño-Díez and Zanetti, 2019; Pyle and Zanetti, 2021; Wan and Briggs, 2016).

In comparison to SPA, sub-tomogram averaging (STA) represents a relatively newer approach in the field. Several intricacies render STA a more complex method, and its widespread application remains confined to a selected number of expert research teams. These challenges include: i) cryo-ET samples, typically thicker than those used in SPA, result in a significantly lower signal-to-noise ratio, posing difficulties in accurately extracting subvolumes; ii) samples for cryo-ET are often more heterogeneous than purified proteins, complicating the alignment and averaging procedures; iii) the required software programs continue to undergo development and must be customized to suit working with protein types. This adaptation is particularly challenging when dealing with proteins lacking well-defined geometries and exhibiting low symmetry, as established software tools may not be readily applicable; iv) while there is evidence that STA can achieve resolution on par with SPA for large and

well-structured proteins like apoferritin, it frequently falls short of providing atomic-level protein details (Tegunov et al., 2021). Consequently, the interpretation of cryo-ET results frequently necessitates combination with complementary techniques, such as comparing various protein constructs, employing structure prediction, and conducting molecular dynamics simulations, to attribute precise molecular identities and interactions within the sub-volumes (Table 1).

When dealing with MCS, cryo-ET faces challenges arising from the proteins' diminutive size, resulting in a weak signal in tomograms, as well as their intrinsic flexibility and limited cellular abundance (Table 2).

### *In Vitro Reconstituted Membrane Contact Site: VAP-A-OSBP*

The molecular organization of in vitro MCS formed by the VAP-A and OSBP complexes has been investigated using cryo-ET and STA (de la Mora et al., 2021). VAP-A is an ER-transmembrane protein known for its recognition of over 100 proteins containing FFAT (two phenylalanines in an acidic track) or FFAT-like amino acid sequences (Di Mattia et al., 2018; Murphy and Levine, 2016). These proteins include various lipid transfer proteins, among them OSBP, responsible for transferring cholesterol synthesized in the ER to the trans-Golgi network (TGN). OSBP comprises an N-terminal PH domain, a central FFAT motif, and a C-terminal lipid transport (ORD) domain.

Complete VAP-A, OSBP, and (1-408)-OSBP (NPHFFAT), a construct lacking the ORD domain, used for studying tethering function, were purified. We designed an in vitro MCS based on a hybrid lipid system, where VAP-A was reconstituted in proteoliposomes in contact with OSBP or (1-408)-OSBP bound to lipidic tubes containing PI4P. This hybrid system was initially designed for VAP-A and OSBP analysis but can be applied to other protein complexes involved in tethering two adjacent membranes. Cryo-EM images of VAP-A at the membrane surface revealed that VAP-A is a flexible molecule with its MSP domain, responsible for binding VAPs partners, capable of extending up to 17 nm and exploring the cytosol. This flexibility allows VAP-A, when in complex with (1-408)-OSBP or OSBP, to form MCS with intermembrane distances spanning from 10 to 30 nm.

The high abundance of protein molecules in this in vitro system enabled the computation of 3D models for VAP-A and N-PH-FFAT at resolutions of 20 Å and 10 Å, respectively. These models revealed a dimeric arrangement for both VAP-A and (1-408)-OSBP. The tethering region of OSBP exhibited a T-shaped configuration with a 14 nm elongated domain parallel to the membrane, a short ~3 nm stem, and PH domains bound to the membrane. Given that the C-terminal region includes a disordered segment of approximately 100 amino acids, which encompasses the FFAT

**Table 2.** Cryo-EM Studies of Membrane Contact Sites and of Constitutive Proteins by SPA and Cryo-ET and STA.

Proteins	Membrane contact sites	Sample preparation	Method of analysis	MCS localization	Protein assignment based on	3D molecular reconstruction
VPS13 (Li et al., 2020)	ER-mitochondria ER-endo/lysosomal system	Soluble 1-1390 VPS13 fragment purified from mammalian cells	SPA	No membrane	Purified proteins	3.75 Å, <i>EMD-21113</i>
ATG2 (Valverde et al., 2019) (Wang et al., 2023)*	ER-lipid droplet ER-autophagosome	Purified protein from mammalian cells	SPA	No membrane	Purified proteins	3D models * of human ATG2A-WIP14 at 3.2 Å resolution and of ATG2A-WIP14-ATG9A complex at 7 Å resolution
Extended synaptotagmin (E-Syst) (Fernández-Busnadiego et al., 2015)	ER-Plasma Membrane	COS-7 cell deposited on cryo-EM grids	In situ Cryo-ET	ER-PM recognizable at the edge of the cell	Deletion of the three E-Syst and overexpression of single E-Syst. Massive formation of ER-PM MCS	nd
VAP-OSBP (de la Mora et al., 2021)	ER-Trans Golgi Network	Purified proteins from <i>E. coli</i> and Sf9 insect cells. In vitro reconstituted MCS	In vitro Cryo-ET and STA	In vitro reconstituted MCS with two different membranes	Sensitivity to calcium Purified protein and hybrid system of VAP-A proteoliposomes and OSBP-bound to PI4P-Galcer lipid nanotubes	3D models of VAP-A at 20 Å resolution (6948 sub-volumes), <i>EMD-11402</i> 3D model of (1-408) OSBP at 9.8 Å resolution (15597 sub-volumes), <i>EMD-11376</i>
Tricalbins (Collado et al., 2019)	ER-Plasma membrane	<i>S. cerevisiae</i> deposited on a cryo-EM grid followed by cryo-FIB milling	In situ Cryo-ET	Recognizable ultrastructure of ER-PM MCS in cryo-tomograms CLEM to locate recognizable region of ER-PM MCS	Deletion of all tethering proteins and expression of single protein of interest	nd 2D averaging
Tricalbins (Hoffmann et al., 2019)	ER-plasma Membrane	cryo-FIB milling	In situ Cryo-ET and 2D averaging			
VPS13C (Cai et al., 2022)	ER-endo/lysosomes	Hela cells deposited on a cryo-EM grid followed by cryo-FIB milling	In situ Cryo-ET and STA	Recognizable ultrastructure after massive formation of ER/endo/lyso MCS by overexpression of VPS13 and Vap-A	Overexpressed proteins bridging ER-endo/lyso MCS Fit of an Alpha Fold model in the EM envelop	47 Å resolution model of VPS13C (576 sub-volumes) <i>EMD-26247</i>

(continued)

Table 2. Continued.

Proteins	Membrane contact sites	Sample preparation	Method of analysis	MCS localization	Protein assignment based on	3D molecular reconstruction
ERMES complex (Wozny et al., 2023)	ER-mitochondria	<i>S. cerevisiae</i> deposited on a cryo-EM grid followed by cryo-FIB milling	In situ Cryo-ET and STA	Cryo-CLEM to locate regions of ER-mitochondria MCS	Endogenous proteins bridging ER-mito MCSs	27 Å resolution model of ERMES complex (1098 sub-volumes) EMD-16872

Abbreviations: SPA, single-particle analysis; cryo-ET, cryo-electron tomography; VAP, vesicle-associated membrane protein-associated protein; OSBP, oxysterol-binding protein; STA, sub-tomogram averaging; MCS, membrane contact sites.

\*Article in BioRxiv, 3D models will be released upon publication.

motif, it suggests that this region can bind two distinct VAP-A dimers located at spatially separated locations. The sequence A362-R408 (47 amino acids), connecting the FFAT motif to the ORD, could potentially extend up to 14 nm, defining the effective range of action of the ORD between the MSP of VAP-A and the two adjacent membranes. This ball-and-chain geometry could facilitate a movement exceeding 20 nm for the ORDs between the ER and TGN membranes, potentially enabling lipid exchange between these compartments.

Further investigation in cells demonstrated that in the absence of its flexible regions, VAP-A, which typically concentrate in ER-Golgi MCS, relocated to ER-mitochondria MCS, likely engaging with VPS13 and PTP51. Notably, this altered ER-mitochondrial localization of VAP-A mutants was primarily associated with sustained interactions with partners residing in mitochondria, rather than being dictated by specific VAP-A length or inter-organelle distances. Consequently, the flexibility of VAP appears to serve as a critical structural component enabling VAP-A to adapt to its binding partners, which exhibit varying turnover rates within the MCS (Subra et al., 2023).

The in vitro reconstitution approach replicates tethering complexes known as MCS and makes them suitable for cryo-ET analysis. These reconstituted MCS exhibit dimensions in the hundreds of nanometers range, like those seen in cellular environments. Notably, the inter-membrane distances within these reconstituted MCS vary from 10 to 30 nanometers, displaying a wider range compared to typical measurements in in situ cryo-ET studies. This variation may arise due to the specific conditions of in vitro reconstituted MCS. Furthermore, it highlights the adaptability of VAP-A, which can adjust its length based on the size of partner proteins it encounters in various MCS within the cell, such as VPS13 and OSBP at ER-mitochondria or ER-TGN sites, respectively. These reconstituted MCS provide a platform for studying the behavior of multiple copies of proteins that tether adjacent membranes, a scenario that is not easily accessible through SPA of isolated proteins. Additionally, this approach offers a simplified environment compared to the in situ approach. By manipulating parameters like protein concentration, partner type, lipid composition, and membrane curvature, the in vitro reconstitution approach facilitates a deeper understanding of the assembly and disassembly mechanisms of MCS. Finally, the substantial number of molecules available for averaging in an in vitro dataset comprising a few dozen up to hundreds of cryo-tomograms, containing the number of protein particles exceeding 10,000 in total, enables the determination of molecular models at sub-nanometer resolution.

### In Situ Cryo-Electron Tomography

Cryo-ET can be used to visualize organelle ultrastructure and proteins in the cellular context. Moreover, it allows for the



examination of organelle interactions, protein-organelle, and protein-protein interactions. In some cases, molecular models of proteins as well as protein complexes could be resolved in situ by means of cryo-ET and STA.

To obtain images with a proper signal-to-noise ratio in cryo-ET, it is essential that the sample's thickness remains below 100–200 nm (Tuijtel et al., 2023). This requirement is met when studying the periphery of eukaryotic cells, which enables the investigation of MCS between the ER and the plasma membrane. However, to study the interior of cells, the sample (cell, tissue, or organoid) is frozen on an EM grid. Subsequently, a cryo-focused ion beam scanning EM (cryo-FIB-SEM) is used to mill the surface of the frozen specimen until a 100–200 nm thick lamella is obtained. This lamella is then imaged using a transmission cryo-EM.

Identifying MCSs within cellular lamellae pose challenges in the absence of protein labels recognizable in cryo-ET. This usually requires CLEM approaches. This technique involves two steps: imaging fluorescent proteins expressed in cell that are deposited on an EM grid to localize the region of interest followed by imaging this same region by cryo-EM.

Several CLEM techniques are available for both room temperature (RT) and frozen samples, as reviewed In the case of membrane architectures by Ganeva and Kukulski (Ganeva and Kukulski, 2020). By conducting CLEM at RT followed by HPF fixation and sectioning, proteins within certain MCSs can be identified, as shown e.g., VPS13 proteins at the ER-late endosomes or the ER-mitochondria contact sites (Kumar et al., 2018) or MOPD2 at the ER-lipid droplet contact sites (Zouiouich et al., 2022). This approach also revealed how the morphology of yeast cortical ER changed with the type of tethering proteins (Hoffmann et al., 2019).

In contrast, cryo-CLEM of cryo-lamellae enables fluorescence microscopy while preserving them in a vitreous state. Established protocols for freezing cells and imaging cryo-lamellae using modified optical microscopes, followed by transfer to cryo-microscopes, have been described (Bieber et al., 2022; Fung et al., 2022). Despite technical complexities, vitreous ice preservation allowed direct visualization of proteins in cryo-tomograms, as seen for example with the ERMES complex at ER-mitochondria contact sites, where the corresponding molecular models were computed by STA (Wozny et al., 2023). Fluorescence localization is largely constrained by the diffraction limit. Efforts in super-resolution light microscopy of frozen samples have provided images of mammalian cell cytoskeleton and organelles, though not yet contact sites (Tuijtel et al., 2019). Alternatively, fluorescent genetically encoded multimeric proteins (GEMs) have been developed to target GFP-labeled proteins. Indeed, GEMs were detectable in cryo-tomograms by their 25 nm icosahedral shape allowing an easier localization of target protein as shown for seipins at ER-lipid droplet contact sites (Fung et al., 2022).

In the regions of contact between membranes, the electron densities that connect adjacent membranes are typically weak in intensity. The presence of multiple proteins with redundancy in their functions adds complexity to the preparation of samples and poses challenges in precisely attributing these electron densities. For example, in yeast, there are six different proteins found at the ER-plasma MCS, while in human cells, VAP-A is known to interact with at least OSBP and CERT at the ER-Golgi contact site (Collado et al., 2019; Hoffmann et al., 2019; Subra, Antonny and Mesmin, 2023). Consequently, unambiguously assigning these protein densities becomes a challenging task. As a common strategy, researchers often resort to removing all potential tethering proteins and subsequently expressing only the protein of interest to facilitate the analysis.

Lastly, the limited number of endogenous proteins within MCS available for averaging restricts the achievable resolution of computed 3D molecular models. Protein overexpression can increase the number of proteins for averaging but may also alter the organelle's ultrastructure.

### *Cryo-ET at Cell Periphery: Extended-Synaptotagmin Within the ER-Plasma Membrane Contact Site*

The initial in situ exploration of MCS focused on the structural analysis of those mediated by extended synaptotagmin (E-syt) proteins (Fernández-Busnadiego et al., 2015). E-syt are proteins anchored in the ER and feature a synaptotagmin mitochondrial lipid binding protein (SMP) domain along with either five C2 domains (E-syt1) or three C2 domains (E-Syt 2/3). E-syt proteins are recognized for their tethering ability, primarily attributed to the C2 domains' capacity to bind phosphatidylinositol 4,5-bisphosphate (PI(4,5)P<sub>2</sub>) present in the plasma membrane, a process regulated by the accumulation of cytosolic calcium. The first cryo-electron tomograms of these MCS were acquired at the periphery of naïve COS-7 cells, but the protein densities observed were too sparse to be definitively assigned to E-Syt proteins. Therefore, it was necessary to induce the substantial formation of these ER-plasma membrane E-Syt contacts through the overexpression of each E-syt individually, in the presence or absence of calcium, to gain insights into the architectural organization of these MCS. Across all E-Syt variants, the ER membrane and the plasma membrane were separated by approximately 18–20 nm. Notably, the distance between membranes was shorter in E-syt1-mediated contacts when exposed to elevated cytosolic calcium concentrations. These observations contributed to the understanding of the calcium-dependent binding behavior of the C2 domain in E-Syt1 relative to E-Syt2/3 and the assignment of an intermediate density to the SMP domain. However, the signal-to-noise ratio of the protein was insufficient for the generation of

a 3D molecular model through subtomogram averaging. Hence, proposing a transport model involving a shuttle or channel remained challenging.

### *Cryo-ET of Yeast ER-Plasma Contact Site: Tricalbins*

Two cryo-ET studies have provided insights into the ER-plasma membrane MCS in the budding yeast (Collado et al., 2019; Hoffmann et al., 2019). The ER in yeast is referred to as the cortical ER (cER), it envelopes up to 30% of the plasma membrane surface. The following six proteins have been found to be involved in these MCS: Scs2, Scs2.2 which are orthologs of mammalian VAP, Ists2, and three tricalbins (Tcb1, Tcb2, Tcb3), which correspond to extended-synaptotagmin orthologs. Tcb 1-3 proteins comprise an SMP domain capable of harboring lipids and four to six C2 domains, some of which can bind to membrane phospholipids.

The ER-PM contact regions' ultrastructure was investigated through two distinct methods: CLEM of resin-embedded cells as conducted by Hoffmann et al. in 2019, and direct in situ cryo-ET as explored by Collado et al. in 2019. These studies unveiled a heterogeneous landscape, characterized by a combination of planar sheets and tubular structures of the cortical ER (cER), particularly within the wild-type (WT) strain. Upon the complete removal of all bridging proteins and the subsequent expression of a single type of protein, noteworthy structural changes were observed. Specifically, the cER predominantly exhibited a tubular configuration when Tcb 1-3 proteins were present, whereas the presence of Scs2 and Ists2 led to the formation of cER sheets. This alteration in morphology suggested that proteins in the WT strain tend to accumulate within regions of the cER characterized by specific curvature. Interestingly, regardless of the type of bridging proteins involved, the distances between the ER and plasma membranes exhibited relative constancy, with an average separation of approximately  $23 \pm 5$  nm. However, it is important to note that these distances did show specificity in the context of various ER-organelle MCS. For instance, in the case of ER-Mitochondria contacts, the distances were found to be approximately  $16 \pm 7$  nm.

In strains where five proteins were depleted and Tcb3 was overexpressed, distinct structural changes were observed in the cER membrane. As shown by Collado et al. (2019), the cER membrane exhibited peaks with diameters of approximately 10 nm. In another study by Hoffmann et al. (2019), the cER membrane displayed a bending or buckling tendency towards the plasma membrane. A quantitative model was developed, predicting that the pronounced curvature of the membrane, as seen in the 10 nm peaks, could substantially reduce the entropy barrier associated with lipid extraction. This reduction in the entropy barrier was estimated to increase the extraction

rate by approximately 500-fold, as outlined in the study by Collado et al. (2019). Furthermore, Hoffmann et al. (2019) reported electron densities representing proteins that spanned both membranes, resembling rigid rods with a length of approximately 20 nm. However, the analysis was limited due to a low signal-to-noise ratio that only 2D projections could be effectively generated. Nevertheless, the 2D classes revealed variability in the tilt angles of these rods, with some tilting up to 20 degrees concerning the cER membrane. This variability suggested the presence of potential flexible protein domains at the membrane anchor. Notably, this observed structure does not align with the assumption that the SMP dimer is organized in parallel to the membrane, shuttling between the two membranes. Instead, it supports a lipid tunneling model as a more fitting explanation.

### *Cryo-ET of ER/Endosome/Lysosome Contact Sites: VPS13C*

Cryo-lamellae of HeLa cells were used to investigate ER-endosome/lysosome MCS containing VPS13C (Cai et al., 2022). VPS13C functions as a lipid transport protein within these MCS. Initially, the presence of VPS13C at ER-endosome/lysosome MCS was detected through fluorescence microscopy of cells. Subsequently, the identification of the areas of interest within the cryo-lamella was facilitated by the substantial expansion of the ER towards endo/lysosomes following the overexpression of the VPS13C and VAP-A tethering complexes. Confirmation of the assignment was achieved using a truncated form of VPS13C. The intermembrane space between these structures was approximately 29 nm, but this distance decreased to around 24 nm with the VPS13C  $\Delta 1,235-1,748$  construct. Notably, rod-like structures with the anticipated length of VPS13C were observed bridging the adjacent membranes. The application of subtomogram averaging resulted in the generation of a low-resolution map, with a resolution of 47 Å, depicting a featureless rod-shaped protein. This model was subsequently fitted with a predicted model of the full-length protein obtained using Alpha Fold-based tools. An intriguing observation was the absence of protein density at the ER/protein interface. This lack of electron density might be explained by several hypothesis: the presence of a flexible domain within this region of VPS13C, the flexibility of the link region between the MSP domain of Vap able to bind VPS13 and the rest of the protein (de la Mora et al., 2021) or the presence of non-overexpressed unknown protein. In the absence of overexpression, intermembrane distances between the ER and endo/lysosomes displayed greater variability, and few, if any, tethering proteins were visibly present. Overall, this study offered compelling evidence that VPS13C possesses structural characteristics conducive to a bridge model for lipid transport.

## Cryo-ET of ER-Mitochondria Contact Sites : ERMES complex

The structural arrangement of the ERMES complex, which plays a pivotal role in facilitating the transport of phospholipids between the membranes of the ER and mitochondria in yeast, was examined using in situ cryo-ET (Wozny et al., 2023). The ERMES complex comprises four distinct proteins: Mmm1, Mdm12, Mdm34, and Mdm10. Mdm10 is a transmembrane protein found in the mitochondrial outer membrane, whereas Mmm1 is integrated into the ER membrane. Mmm1, Mdm12, and Mdm34 share a conserved SMP domain.

The identification of contact zones within the cryo-lamellae was achieved through cryo-CLEM using mdm34-mNeon green. These contact regions exhibited a surface area of approximately  $0.02 \mu\text{m}^2$ , and the intermembrane separation between the ER and mitochondria remained relatively constant at  $\sim 20\text{--}25 \text{ nm}$ . Notably, the ER membrane involved in the contact displayed no specific curvature, nor did it adopt concave, convex, or flat configurations. Electron densities corresponding to proteins bridging the adjacent membranes were visible by eye. Additionally, these protein densities were consistently arranged in clusters without direct contact, indicating a spatial organization potentially influenced by proteins shared between the two organelles that orchestrate the clustering of ERMES complexes.

A 3D molecular model was generated from 1098 subvolumes, albeit at a resolution of  $27 \text{ \AA}$ , which precluded the construction of a secondary structure model. Therefore, an atomic model was assembled by amalgamating existing protein information, such as the localization of Mmm1 in the mitochondrial outer membrane and its interaction with Mdm12, with a 3D model derived from predictions employing Alpha Fold-based tools. This hybrid model was then optimized via atomistic molecular dynamics based flexible fitting and fitted into the EM envelope. The resulting 3D model unveiled the organization of the four subunits in the order of Mmm1-Mdm12, Mdm34, and Mmm10, which bridge the two membranes connecting the ER to the mitochondria, adopting a zigzag configuration. Importantly, this 1:1:1 protein/complex stoichiometry validated the quantitative fluorescence microscopy yielded findings. Molecular modeling indicated that the interior of the SMP domains possesses hydrophobic properties, suggesting that they have the potential to accommodate phospholipids. This lends support to a model of unidirectional lipid transfer between the ER and mitochondria through a protein conduit, rather than a shuttle mechanism.

This comprehensive study combined cutting-edge methodologies including quantitative fluorescence microscopy, in situ cryo-ET, and atomistic molecular dynamics to offer novel insights into the structural organization of the ERMES complex at ER-mitochondrial contact sites, spanning from the molecular to cellular scales. It is worth

highlighting that the study was conducted using endogenous ERMES complexes within wild-type cells, without the need for protein overexpression. This represents a groundbreaking contribution to our understanding of the ERMES complex and, by extension, other MSCs in general.

## Conclusion

Recent studies have highlighted the application and merits of cryo-EM for exploring structural characteristics of MCS. Cryo-EM provides a versatile perspective, spanning from the molecular to cellular levels, encompassing the 10 nm to 500 nm scale—a range not easily explored through alternative biological approaches. Additionally, cryo-EM can be effectively combined with other techniques to generate low-resolution EM maps, particularly for highly flexible domains, such as molecular dynamics, fluorescence microscopy, or scattering methods (Yu et al., 2023). Recent advancements in time-resolved cryo-EM have facilitated the elucidation of complex formation kinetics and the visualization of transient conformations (Torino et al., 2023).

Expected advancements in cryo-ET of MCS in cellular contexts hold promise as ongoing endeavors tackle inherent obstacles. Innovative instruments are being developed to ensure consistent lamellae preparation and to acquire high-quality tomographic data. New strategies, such as cryo-CLEM paired with super-resolution techniques (Ganeva and Kukulski, 2020), genetically encoded multi-meric particle-based protein localization (Fung et al., 2022), and deep learning approaches applied to annotated cryo-tomograms, enable improved recognition of proteins within cryo-lamellae (de Teresa-Trueba et al., 2023).

A pivotal issue lies in the limited availability of endogenous proteins for generating 3D models. While protein overexpression is an option, it can substantially alter organelle ultrastructure. To mitigate this, efforts are being made to accelerate cryo-ET data collection, reducing acquisition times from approximately 30 to about 5 min per tilt series (Eisenberg-Bord et al., 2016). This development is expected to significantly increase the number of subtomograms available for averaging. Coupled with new denoising algorithms and 3D classification techniques, it becomes feasible to analyze a greater range of endogenous proteins (Zivanov et al., 2022b).

Cryo-ET analysis of purified organelles has yet to be experimented for studying MCS, although it is feasible to image a greater number of such structures on a grid compared to cells, and cryo-FIB milling is not necessary. Successful applications of this approach include investigations into the role of mitofusin in mitochondria fusion (Brandt et al., 2016), determination of the structure of the Ryanodine receptor within ER vesicles (Chen and Kudryashev, 2020), and examination of the ribosome-translocon on ER vesicles (Gemmer et al., 2023). However, realizing this potential

will likely necessitate investments in new organelle purification methods.

Combining cryo-EM and in vitro reconstitution of MCS using purified proteins enables the investigation of queries that are beyond the reach of cellular studies. This approach also facilitates the generation of 3D protein models at a high, potentially atomic resolution. The roster of proteins affiliated with MCS within cells is notably expanding, with many of them poised as promising candidates for comprehensive exploration and the elucidation of their functional mechanisms upon successful purification.

Abbreviations: three-dimensional (3D), cryo-electron microscopy (cryo-EM), cryo-electron tomography (cryo-ET), single particle analysis (SPA), sub-tomogram averaging (STA), endoplasmic reticulum (ER), vesicle-associated membrane protein-associated protein (VAP), correlative light-electron microscopy (CLEM), membrane contact sites (MCS).




### Declaration of Conflicting Interests

The authors declared no potential conflicts of interest with respect to the research, authorship, and/or publication of this article.

### Funding

The authors disclosed receipt of the following financial support for the research, authorship, and/or publication of this article: This work was supported by the Agence Nationale de la Recherche, (grant number ANR-21-CE13-0021-01, ANR10-INBS-04).

### ORCID iDs

Cyan Ching  <https://orcid.org/0000-0002-2519-7490>  
Daniel Lévy  <https://orcid.org/0000-0002-8949-4072>  
Manuela Dezi  <https://orcid.org/0000-0001-8727-9910>

### References

- Adlakha J, Hong Z, Li P, Reinisch K (2022). Structural and biochemical insights into lipid transport by VPS13 proteins. *The Journal of Cell Biology* 221(5), e202202030. doi: 10.1083/jcb.202202030
- Balyschew N, Yushkevich A, Mikirtumov V, Sanchez RM, Sprink T, Kudryashev M (2023). Streamlined structure determination by cryo-electron tomography and subtomogram averaging using TomoBEAR. *Nature Communications* 14(1), 1. Nature Publishing Group: 6543. doi: 10.1038/s41467-023-42085-w
- Bernhard W, Rouiller C (1956). Close topographical relationship between mitochondria and ergastoplasm of liver cells in a definite phase of cellular activity. *The Journal of Biophysical and Biochemical Cytology* 2(4 Suppl), 73–78. doi: 10.1083/jcb.2.4.73
- Bertin A, de Franceschi N, de la Mora E, Maity S, Alqabandi M, Miguet N, di Cicco A, Roos WH, Mangenot S, Weissenhorn W, Bassereau P (2020). Human ESCRT-III polymers assemble on positively curved membranes and induce helical membrane tube formation. *Nature Communications* 11(1), 2663. doi: 10.1038/s41467-020-16368-5
- Bieber A, Capitanio C, Erdmann PS, Fiedler F, Beck F, Lee CW, Li D, Hummer G, Schulman BA, Baumeister W, Wilfling F. (2022). In situ structural analysis reveals membrane shape transitions during autophagosome formation. *Proceedings of the National Academy of Sciences of the United States of America* 119(39), e2209823119. <https://doi.org/10.1073/pnas.2209823119>
- Brandt T, Cavellini L, Kühlbrandt W, Cohen MM. (2016). A mitofusin-dependent docking ring complex triggers mitochondrial fusion in vitro. *eLife* 5, e14618. <https://doi.org/10.7554/eLife.14618>
- Cai S, Wu Y, Guillén-Samander A, Hancock-Cerutti W, Liu J, De Camilli P. (2022). In situ architecture of the lipid transport protein VPS13C at ER-lysosome membrane contacts. *Proceedings of the National Academy of Sciences of the United States of America* 119(29), e2203769119. <https://doi.org/10.1073/pnas.2203769119>
- Castaño-Díez D, Zanetti G (2019). In situ structure determination by subtomogram averaging. *Current Opinion in Structural Biology* 58, 68–75. <https://doi.org/10.1016/j.sbi.2019.05.011>
- Chen W, Kudryashev M (2020). Structure of RyR1 in native membranes. *EMBO reports* 21(5), e49891. <https://doi.org/10.15252/embr.201949891>
- Cheng J, Wu C, Li J, Yang Q, Zhang X (2023). Visualizing translating dynamics in situ at high spatial and temporal resolution in eukaryotic cells. *bioRxiv*. Available at: <https://www.biorxiv.org/content/10.1101/2023.07.12.548775v1> (accessed 6 December 2023).
- Collado J, Kalemánov M, Campelo F, Bourgoint C, Thomas F, Loewith R, Martínez-Sánchez A, Baumeister W, Stefan CJ, Fernández-Busnadiego R. (2019). Tricalbin-mediated contact sites control ER curvature to maintain plasma membrane integrity. *Developmental Cell* 51(4), 476–487.e7. <https://doi.org/10.1016/j.devcel.2019.10.018>
- Daniele T, Hurbain I, Vago R, Casari G, Raposo G, Tacchetti C, Schiaffino MV. (2014). Mitochondria and melanosomes establish physical contacts modulated by Mfn2 and involved in organelle biogenesis. *Current Biology: CB* 24(4), 393–403. <https://doi.org/10.1016/j.cub.2014.01.007>
- Daurly L, Orange F, Taveau JC, Verchère A, Monlezun L, Gounou C, Marreddy RKR, Picard M, Broutin I, Pos KM, Lambert O. (2016). Tripartite assembly of RND multidrug efflux pumps. *Nature Communications*, 7, Article number: 10731. <http://dx.doi.org/10.1038/ncomms10731>
- de la Mora E, Dezi M, Di Cicco A, Bigay J, Gautier R, Manzi J, Polidori J, Castaño-Díez D, Mesmin B, Antonny B, Lévy D. (2021). Nanoscale architecture of a VAP-A-OSBP tethering complex at membrane contact sites. *Nature Communications* 12(1), 3459. <https://doi.org/10.1038/s41467-021-23799-1>
- de Teresa-Trueba I, Goetz SK, Mattausch A, Stojanovska F, Zimmerli CE, Toro-Nahuelpan M, Cheng DWC, Tollervey F, Pape C, Beck M, et al. (2023). Convolutional networks for supervised mining of molecular patterns within cellular context. *Nature Methods* 20(2), 284–294. <https://doi.org/10.1038/s41592-022-01746-2>
- Di Mattia T, Wilhelm LP, Ikhlef S, Wendling C, Spehner D, Nominé Y, Giordano F, Mathelin C, Drin G, Tomasetto C, Alpy F. (2018). Identification of MOSPD2, a novel scaffold for endoplasmic reticulum membrane contact sites. *EMBO reports* 19(7), e45453. <https://doi.org/10.15252/embr.201745453>

- Eisenberg-Bord M, Shai N, Schuldiner M, Bohnert M. (2016). A tether is a tether is a tether: tethering at membrane contact sites. *Developmental Cell* 39(4), 395–409. <https://doi.org/10.1016/j.devcel.2016.10.022>
- Fernández-Busnadiego R, Saheki Y, De Camilli P (2015). Three-dimensional architecture of extended synaptotagmin-mediated endoplasmic reticulum-plasma membrane contact sites. *Proceedings of the National Academy of Sciences of the United States of America* 112(16), E2004–E2013.
- Fung HK, Hayashi Y, Salo VT, Babenko A, Zagoriy I, Brunner A, Ellenberg J, Müller CW, Cuylen-Haering S, Mahamid J, et al. (2022). Genetically encoded multimeric tags for intracellular protein localisation in cryo-EM. *bioRxiv*. Available at: <https://www.biorxiv.org/content/10.1101/2022.12.10.519870v1> (accessed 8 August 2023).
- Ganeva I, Kukulski W (2020). Membrane architecture in the spotlight of correlative microscopy. *Trends in Cell Biology* 30(7), 577–587. <https://doi.org/10.1016/j.tcb.2020.04.003>
- Gemmer M, Chaillet ML, van Loenhout J, Cuevas Arenas R, Vismpas D, Gröllers-Mulderij M, Koh FA, Albanese P, Scheltema RA, Howes SC, et al. (2023). Visualization of translation and protein biogenesis at the ER membrane. *Nature* 614(7946), 160–167. <https://doi.org/10.1038/s41586-022-05638-5>
- Guyard V, Monteiro-Cardoso VF, Omrane M, Sauvanet C, Houcine A, Boulogne C, Ben Mbarek K, Vitale N, Faklaris O, El Khallouki N, et al. (2022). ORP5 and ORP8 orchestrate lipid droplet biogenesis and maintenance at ER-mitochondria contact sites. *The Journal of Cell Biology* 221(9), e202112107. <https://doi.org/10.1083/jcb.202112107>
- Hoffmann PC, Bharat TAM, Wozny MR, Boulanger J, Miller EA, Kukulski W, et al. (2019). Tricalbins contribute to cellular lipid flux and form curved ER-PM contacts that are bridged by rod-shaped structures. *Developmental Cell* 51(4), 488–502.e8. <https://doi.org/10.1016/j.devcel.2019.09.019>
- Hoffmann PC, Giandomenico SL, Ganeva I, Wozny MR, Sutcliffe M, Lancaster MA, Kukulski W, et al. (2021). Electron cryotomography reveals the subcellular architecture of growing axons in human brain organoids. *eLife* 10, e70269. <https://doi.org/10.7554/eLife.70269>
- Hutchings J, Stancheva VG, Brown NR, Cheung ACM, Miller EA, Zanetti G, et al. (2021). Structure of the complete, membrane-assembled COPII coat reveals a complex interaction network. *Nature Communications* 12(1), 2034. <https://doi.org/10.1038/s41467-021-22110-6>
- Jamecna D, Polidori J, Mesmin B, Dezi M, Levy D, Bigay J, Antonny B, et al. (2019). An intrinsically disordered region in OSBP acts as an entropic barrier to control protein dynamics and orientation at membrane contact sites. *Developmental Cell* 49(2), 220–234.e8. <https://doi.org/10.1016/j.devcel.2019.02.021>
- Kaipa JM, Krasnoselska G, Owens RJ, van den Heuvel J. (2023). Screening of membrane protein production by comparison of transient expression in insect and mammalian cells. *Biomolecules* 13(5), 817. <https://doi.org/10.3390/biom13050817>
- Kovtun O, Leneva N, Bykov YS, Ariotti N, Teasdale RD, Schaffer M, Engel BD, Owen DJ, Briggs JAG, Collins BM, et al. (2018). Structure of the membrane-assembled retromer coat determined by cryo-electron tomography. *Nature* 561(7724), 561–564.
- Kudryashev M, Castaño-Díez D, Deluz C, Hassaine G, Grasso L, Graf-Meyer A, Vogel H, Stahlberg H, et al. (2016). The structure of the mouse serotonin 5-HT<sub>3</sub> receptor in lipid vesicles. *Structure* 24(1), 165–170. <https://doi.org/10.1016/j.str.2015.11.004>
- Kumar N, Leonzino M, Hancock-Cerutti W, Horenkamp FA, Li P, Lees JA, Wheeler H, Reinisch KM, De Camilli P, et al. (2018). VPS13A And VPS13C are lipid transport proteins differentially localized at ER contact sites. *Journal of Cell Biology* 217(10), 3625–3639. <https://doi.org/10.1083/jcb.201807019>
- Li M, Tripathi-Giesgen I, Schulman BA, Baumeister W, Wilfling F, et al. (2023). In situ snapshots along a mammalian selective autophagy pathway. *Proceedings of the National Academy of Sciences of the United States of America* 120(12), e2221712120. <https://doi.org/10.1073/pnas.2221712120>
- Li P, Lees JA, Lusk CP, Reinisch KM (2020). Cryo-EM reconstruction of a VPS13 fragment reveals a long groove to channel lipids between membranes. *The Journal of Cell Biology* 219(5), e202001161. <https://doi.org/10.1083/jcb.202001161>
- Mesmin B, Bigay J, Moser von Filseck J, Lacas-Gervais S, Drin G, Antonny B, et al. (2013). A four-step cycle driven by PI(4)P hydrolysis directs sterol/PI(4)P exchange by the ER-Golgi tether OSBP. *Cell* 155(4), 830–843. <https://doi.org/10.1016/j.cell.2013.09.056>
- Murphy SE, Levine TP (2016). VAP, a versatile access point for the endoplasmic reticulum: review and analysis of FFAT-like motifs in the VAPome. *Biochimica Et Biophysica Acta* 1861(8 Pt B), 952–961. <https://doi.org/10.1016/j.bbali.2016.02.009>
- Notti RQ, Walz T (2022). Native-like environments afford novel mechanistic insights into membrane proteins. *Trends in Biochemical Sciences* 47(7), 561–569. <https://doi.org/10.1016/j.tibs.2022.02.008>
- Obr M, Hagen WJH, Dick RA, Yu L, Kotecha A, Schur FKM (2022). Exploring high-resolution cryo-ET and subtomogram averaging capabilities of contemporary DEDs. *Journal of Structural Biology* 214(2), 107852. <https://doi.org/10.1016/j.jsb.2022.107852>
- Pfeffer S, Mahamid J (2018). Unravelling molecular complexity in structural cell biology. *Current Opinion in Structural Biology* 52, 111–118. <https://doi.org/10.1016/j.sbi.2018.08.009>
- Pyle E, Zanetti G (2021). Current data processing strategies for cryo-electron tomography and subtomogram averaging. *The Biochemical Journal* 478(10), 1827–1845. <https://doi.org/10.1042/BCJ20200715>
- Saibil HR (2022). Cryo-EM in molecular and cellular biology. *Molecular Cell* 82(2), 274–284. <https://doi.org/10.1016/j.molcel.2021.12.016>
- Sari D, Gupta K, Raj DBTG, Aubert A, Drncová P, Garzoni F, Fitzgerald D, Berger I. (2016). The multiBac baculovirus/insect cell expression vector system for producing complex protein biologics. *Advances in Experimental Medicine and Biology* 896, 199–215. [https://doi.org/10.1007/978-3-319-27216-0\\_13](https://doi.org/10.1007/978-3-319-27216-0_13)
- Scorrano L, De Matteis MA, Emr S, Giordano F, Hajnóczky G, Kommann B, Lackner LL, Levine TP, Pellegrini L, Reinisch K. (2019). Coming together to define membrane contact sites. *Nature Communications* 10(1), 1287. <https://doi.org/10.1038/s41467-019-09253-3>
- Sorrentino S, Conesa JJ, Cuervo A, Melero R, Martins B, Fernandez-Gimenez E, de Isidro-Gomez FP, de la Morena J, Studt J-D, Sorzano COS. (2021). Structural analysis of receptors and actin polarity in platelet protrusions. *Proceedings of the*

- National Academy of Sciences *118*(37), e2105004118. <https://doi.org/10.1073/pnas.2105004118>
- Subra M, Antony B, Mesmin B (2023). New insights into the OSBP–VAP cycle. *Current Opinion in Cell Biology* *82*, 102172. <https://doi.org/10.1016/j.ceb.2023.102172>
- Subra M, Dezi M, Bigay J, Lacas-Gervais S, Di Cicco A, Araújo ARD, Abélanet S, Fleuriot L, Debayle D, Gautier R, et al. (2023). VAP-A intrinsically disordered regions enable versatile tethering at membrane contact sites. *Developmental Cell* *58*(2), 121–138.e9. <https://doi.org/10.1016/j.devcel.2022.12.010>
- Tegunov D, Xue L, Dienemann C, Cramer P, Mahamid J, et al. (2021). Multi-particle cryo-EM refinement with M visualizes ribosome-antibiotic complex at 3.5 Å in cells. *Nature Methods* *18*(2), 186–193. <https://doi.org/10.1038/s41592-020-01054-7>
- Torino S, Dhurandhar M, Stroobants A, Claessens R, Efremov RG (2023). Time-resolved cryo-EM using a combination of droplet microfluidics with on-demand jetting. *Nature Methods*, *20*(9), 1400–1408. <http://dx.doi.org/10.1038/s41592-023-01967-z>
- Tuijtel MW, Koster AJ, Jakobs S, Faas FGA, Sharp TH (2019). Correlative cryo super-resolution light and electron microscopy on mammalian cells using fluorescent proteins. *Scientific Reports* *9*(1), 1369. <https://doi.org/10.1038/s41598-018-37728-8>
- Tuijtel MW, Kreysing JP, Welsch S, Hummer G, Beck M, Turoňová B (2023). Thinner is not always better: Optimising cryo lamellae for subtomogram averaging. *bioRxiv*. Available at: <https://www.biorxiv.org/content/10.1101/2023.07.31.551274v1> (accessed 22 December 2023).
- Uchański T, Masiulis S, Fischer B, Kalichuk V, López-Sánchez U, Zarkadas E, Weckener M, Sente A, Ward P, Wohlkönig A. (2021). Megabodies expand the nanobody toolkit for protein structure determination by single-particle cryo-EM. *Nature Methods* *18*(1), 60–68. <https://doi.org/10.1038/s41592-020-01001-6>
- Valverde DP, Yu S, Boggavarapu V, Kumar N, Lees JA, Walz T, Reinisch KM, Melia TJ (2019). ATG2 transports lipids to promote autophagosome biogenesis. *The Journal of Cell Biology* *218*(6), 1787–1798. <https://doi.org/10.1083/jcb.201811139>
- Venditti R, Rega LR, Masone MC, Santoro M, Polishchuk E, Sarnataro D, Paladino S, D’Auria S, Varriale A, Olkkonen VM, et al. (2019). Molecular determinants of ER–Golgi contacts identified through a new FRET–FLIM system. *Journal of Cell Biology* *218*(3), 1055–1065. <https://doi.org/10.1083/jcb.201812020>
- Wan W, Briggs J (2016). Cryo-electron tomography and subtomogram averaging. *Methods in Enzymology* *579*, 329–367. <https://doi.org/10.1016/bs.mie.2016.04.014>
- Wang Y, Dahmane S, Ti R, Mai X, Zhu L, Carlson L-A, Stjepanovic G (2023). Structural basis for lipid transfer by the ATG2A–ATG9A complex. *bioRxiv*. Available at: <https://www.biorxiv.org/content/10.1101/2023.07.08.548186v1> (accessed 6 December 2023).
- Wang Z, Grange M, Pospich S, Wagner T, Kho AL, Gautel M, Raunser S, et al. (2022). Structures from intact myofibrils reveal mechanism of thin filament regulation through nebulin. *Science* *375*(6582), eabn1934. <https://doi.org/10.1126/science.abn1934>
- Wozny MR, Di Luca A, Morado DR, Picco A, Khaddaj R, Campomanes P, Ivanović L, Hoffmann PC, Miller EA, Vanni S, Kukulski W, et al. (2023). In situ architecture of the ER-mitochondria encounter structure. *Nature* *618*(7963), 188–192. <https://doi.org/10.1038/s41586-023-06050-3>
- Xing H, Taniguchi R, Khusainov I, Kreysing JP, Welsch S, Turoňová B, Beck M, et al. (2023). Translation dynamics in human cells visualized at high resolution reveal cancer drug action. *Science* *381*(6653), 70–75. <https://doi.org/10.1126/science.adh1411>
- Yip KM, Fischer N, Paknia E, Chari A, Stark H, et al. (2020). Atomic-resolution protein structure determination by cryo-EM. *Nature* *587*(7832), 157–161. <https://doi.org/10.1038/s41586-020-2833-4>
- Young LN, Villa E (2023). Bringing structure to cell biology with cryo-electron tomography. *Annual Review of Biophysics* *52*, 573–595. <https://doi.org/10.1146/annurev-biophys-111622-091327>
- Yu M, Heidari M, Mikhaleva S, Tan PS, Mingu S, Ruan H, Reinkemeier CD, Obarska-Kosinska A, Siggel M, Beck M, et al. (2023). Visualizing the disordered nuclear transport machinery in situ. *Nature* *617*(7959), 162–169. <https://doi.org/10.1038/s41586-023-05990-0>
- Zhang X, Sridharan S, Zagoriy I, Eugster Oegema C, Ching C, Pflaesterer T, Fung HKH, Becher I, Poser I, Müller CW, et al. (2023). Molecular mechanisms of stress-induced reactivation in mumps virus condensates. *Cell* *186*(9), 1877–1894.e27. <https://doi.org/10.1016/j.cell.2023.03.015>
- Zivanov J, Otón J, Ke Z, von Kügelgen A, Pyle E, Qu K, Morado D, Castaño-Díez D, Zanetti G, Bharat TA, et al. (2022a). A Bayesian approach to single-particle electron cryo-tomography in RELION-4.0. *eLife* *11*, e83724. <https://doi.org/10.7554/eLife.83724>
- Zivanov J, Otón J, Ke Z, von Kügelgen A, Pyle E, Qu K, Morado D, Castaño-Díez D, Zanetti G, Bharat TA, et al. (2022b). A Bayesian approach to single-particle electron cryo-tomography in RELION-4.0. *eLife* *11*, e83724. <https://doi.org/10.7554/eLife.83724>
- Zouiouich M, Di Mattia T, Martinet A, Eichler J, Wendling C, Tomishige N, Grandgirard E, Fuggetta N, Fromental-Ramain C, Mizzon G. (2022). MOSPD2 Is an endoplasmic reticulum–lipid droplet tether functioning in LD homeostasis. *Journal of Cell Biology* *221*(6), e202110044. <https://doi.org/10.1083/jcb.202110044>